


On the occurrence of stellar fission in binary-driven hypernovae

S. R. ZHANG (张书瑞) ^{1, 2, 3} AND R. RUFFINI ^{1, 4, 5}¹*ICRANet, Piazza della Repubblica 10, I-65122 Pescara, Italy*²*School of Astronomy and Space Science, University of Science and Technology of China, Hefei 230026, China*³*CAS Key Laboratory for Research in Galaxies and Cosmology, Department of Astronomy, University of Science and Technology of China, Hefei 230026, China*⁴*ICRA, Dipartimento di Fisica, Sapienza Università di Roma, P.le Aldo Moro 5, I-00185 Rome, Italy*⁵*INAF, Viale del Parco Mellini 84, I-00136 Rome, Italy*

ABSTRACT

The binary-driven hypernova (BdHN) model address long gamma-ray bursts (GRBs) associated with type Ic supernovae (SNe) through a series of physical episodes that occur in a binary composed of a carbon-oxygen (CO) star (of mass $\sim 10M_{\odot}$) and a neutron star (NS) companion (of mass $\sim 2M_{\odot}$) in a compact orbit. The SN explosion of the CO star triggers sequence of seven events. The BdHN model has followed the traditional picture of the SN from the CO iron's core collapse. However, the lack of a solution to the problem of producing successful SNe leaves room for alternative scenarios. We here show that tidal synchronization of the CO-NS binary can lead the CO star to critical conditions for fission, hence splitting into two stellar remnants, e.g., $\sim 8.5M_{\odot} + 1.5M_{\odot}$. We give specific examples of the properties of the products for various orbital periods relevant to BdHNe. The astrophysical consequences of this scenario are outlined.

Keywords: Gamma-ray burst — Close binaries — Core-collapse supernovae — Neutron stars — Black holes

1. INTRODUCTION

The origin of long gamma-ray bursts (GRBs) is thought to be related to the death of massive stars, being their association with type Ic supernovae (SNe) Galama et al. (1998); Woosley & Bloom (2006); Della Valle (2011); Hjorth & Bloom (2012) one of the most compiling observational evidence. Since most massive stars belong to binaries (see, e.g., Kobulnicky & Fryer 2007; Sana et al. 2012), the direct collapse of a massive star to a BH should not produce an SN, observed pre-SN progenitors have masses $\lesssim 18 M_{\odot}$ (Smartt 2009, 2015), and stellar evolution models predict the direct formation of a BH only in progenitor stars $\gtrsim 25M_{\odot}$ (see, e.g., Heger et al. 2003), one can conclude that the GRB and the SN should not originate from a single star.

Based on the above theoretical and observational clues, the binary-driven hypernova (BdHN) model proposes a binary system composed of a carbon-oxygen star (CO) and a neutron star (NS) companion as the progenitor of GRB-SNe. We refer the reader to Rueda & Ruffini (2012); Fryer et al. (2014, 2015); Becerra et al. (2016); Ruffini et al. (2018b,a); Becerra et al. (2019); Ruffini et al. (2019); Rueda & Ruffini (2020); Moradi et al. (2021); Ruffini et al. (2021); Rueda et al. (2022b,a); Wang et al. (2022); Rueda et al. (2022c); Becerra et al. (2022), for theoretical details and applications of the BdHN model to specific sources, and to Aimuratov et al. (2023) for the latest developments.

The BdHN model assumes the occurrence of the SN onsets the entire cataclysmic event: the core collapse of the CO forms a newborn NS (hereafter ν NS) and ejects material that accretes onto the NS companion and the ν NS owing to matter fallback. In this picture, the binary's orbital period is a critical parameter determining the system's fate and energetics, which leads to the classification of BdHNe into type I ($\gtrsim 10^{52}$ erg), II ($\sim 10^{50}$ –

Corresponding author: S. R. Zhang
zhangsr@mail.ustc.edu.cn

ruffini@icra.it

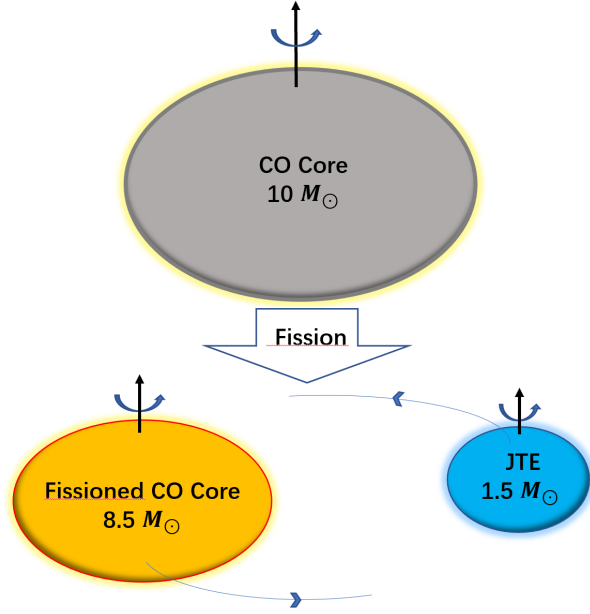


Figure 1. Schematic diagram illustrating the fission of the CO star into the fission CO core and JTE.

10^{52} erg), and III ($\lesssim 10^{50}$ erg; see [Aimuratov et al. 2023](#), for details).

Since the SN trigger and the ν NS formation are crucial in explaining the event, a vast new topic has emerged from studying alternatives to assuming a single non-rotating star core-collapse SN event in the CO core. The alternative scenario has been recently advanced based on the fission process of the CO core due to its high rotation rate gained by corotation with its NS companion. It has been indicated in [Aimuratov et al. \(2023\)](#) that the GRB-SN might be triggered, e.g., by a fast rotating $10M_{\odot}$ CO star set in corotation with a companion NS in an orbital period of a few minutes. The CO fission creates an $8.5M_{\odot}$ Maclaurin ellipsoid core and a $1.5M_{\odot}$ companion triaxial Jacobi ellipsoid (hereafter, JTE) in a Roche-lobe configuration (see Fig. 1).

The aim of this article is to evaluate specific examples of the above fission process. For this task, we have generalized (see appendix A) the classical tables of the Maclaurin and Jacobi sequences in [Chandrasekhar \(1969\)](#); [Jeans \(1929\)](#) treatises necessary to describe the CO core fission in the present astrophysical scenario.

In Section 2, we illustrate a few examples of the binary progenitor before fission, i.e., an initial $10M_{\odot}$ CO core corotating with an NS companion for selected values of the orbital period. Section 3 shows examples of the system after the fission of the initial $10M_{\odot}$ CO core into a Maclaurin new CO core of $8.5M_{\odot}$ and a JTE companion of $1.5M_{\odot}$ (see Fig. 1). Mass and angular

momentum conservation are necessary conditions in the fission process.

To exemplify, we assume the CO core after fission lies on a specific location of the Maclaurin sequence and the JTE, by definition, on the Jacobi sequence. One could select alternative locations for the fission products, and the outcomes would not vary significantly, as the physical quantities are similar. The five examples of fission we are considering are displayed in Tables 1 and 2. Table 1 lists the physical properties of the CO before fission, while Table 2 presents the physical properties of the fission products. The initial CO core in all examples has a mass of $10M_{\odot}$, while the rotation period varies.

2. BEFORE FISSION

Let us assume that the binary consists of a CO core of mass M_{CO} and an NS of mass M_{NS} . The corotation implies the CO's core spin period is the same as the orbit period, P . We denote the rotational angular velocity of the CO core as Ω . The initial CO core is assumed to be at the Maclaurin-Jacobi bifurcation point, at which the angular velocity and density fulfill (see, e.g., [Chandrasekhar 1969](#))

$$\frac{\Omega^2}{\pi G \rho_{\text{CO}}} \approx 0.37423. \quad (1)$$

The rotation angular momentum of the CO core is

$$J_{\text{CO}} = I_{\text{CO}} \Omega, \quad (2)$$

where the moment of inertia is given by

$$I_{\text{CO}} = \frac{2}{5} M_{\text{CO}} a_{\text{CO}}^2, \quad a_{\text{CO}} = \bar{a}_{\text{CO}} (1 - e^2)^{-1/6}, \quad (3)$$

with the reference radius \bar{a} (of the spherical configuration with the same volume) set by

$$\bar{a}_{\text{CO}} = \left(\frac{3M_{\text{CO}}}{4\pi\rho_{\text{CO}}} \right)^{1/3} \approx \left(\frac{3}{4} \frac{0.37423 GM_{\text{CO}}}{\Omega^2} \right)^{1/3}, \quad (4)$$

where in the last expression, we used Eq. (1). Having defined all the above, the angular momentum (2) can be written as

$$J_{\text{CO}} \approx 0.30375 \sqrt{G M_{\text{CO}}^3 \bar{a}_{\text{CO}}}, \quad (5)$$

where we used that the eccentricity is $e \approx 0.812670$ at the bifurcation point. The constants 0.37423 in Eq. (1) and 0.30375 in Eq. (5) are, respectively, the values of the dimensionless square of angular velocity and angular momentum at the Maclaurin-Jacobi bifurcation point, which correspond to the first entry in Tables 3 and 4.

Table 1. The physical quantities before fission. The mass of the CO core is fixed at $10M_\odot$. Unless otherwise specified, we use cgs units. From left to right, the table's columns are the spin period, density, average radius, angular momentum, rotational energy, and moment of inertia of the CO core.

P (min)	ρ (g cm ⁻³)	\bar{a} (cm)	J_{CO} (g cm ² s ⁻¹)	E_k (erg)	I (g cm ²)
110	11.5573	7.43424×10^{10}	6.00045×10^{52}	2.85621×10^{49}	1.09934×10^{56}
90	17.2647	6.50334×10^{10}	5.61221×10^{52}	3.26505×10^{49}	8.4126×10^{55}
40	87.4023	3.78746×10^{10}	4.28292×10^{52}	5.60633×10^{49}	2.85334×10^{55}
20	349.609	2.38595×10^{10}	3.39935×10^{52}	8.89949×10^{49}	1.13235×10^{55}
5	5593.75	9.46866×10^9	2.14146×10^{52}	2.24253×10^{50}	1.78334×10^{54}

3. AFTER FISSION

We turn now to the two systems after the fission process of the original CO core. The products of the process are a new CO core with a mass of M_{COF} and a JTE with a mass of M_{JTE} . This process is shown in Fig. 1. In the fission process, the following conditions are assumed:

- (i) The fission products corotate with the same period (Roche condition);
- (ii) The new CO core is located at a given point of the Maclaurin sequence, and the second product is a JTE, so it lies on the Jacobi sequence (see examples provided below);
- (iii) The mass is conserved, i.e.,

$$M_{\text{CO}} = M_{\text{COF}} + M_{\text{JTE}} \quad (6)$$

- (iv) The angular momentum of the CO core is conserved, i.e.,

$$J_{\text{CO}} = J_{\text{COF}} + J_{\text{JTE}} + J_{\text{orbit}}. \quad (7)$$

In analogy with Eq. (5), the angular momentum of the new CO core can be written as

$$J_{\text{COF}} = I_{\text{COF}} \Omega_f = c_1 \sqrt{G M_{\text{COF}}^3 \bar{a}_{\text{COF}}}, \quad (8)$$

where the reference spherical radius is

$$\bar{a}_{\text{COF}} = \left(\frac{3M_{\text{COF}}}{4\pi\rho_{\text{COF}}} \right)^{1/3} = \left(\frac{3}{4} \frac{c_2 G M_{\text{COF}}}{\Omega_f^2} \right)^{1/3}, \quad (9)$$

and the constant c_2 is defined by

$$\frac{\Omega_f^2}{\pi G \rho_{\text{COF}}} = c_2. \quad (10)$$

Likewise, we define

$$J_{\text{JTE}} = I_{\text{JTE}} \Omega_f = c_3 \sqrt{G M_{\text{JTE}}^3 \bar{a}_{\text{JTE}}}, \quad (11)$$

where

$$\bar{a}_{\text{JTE}} = \left(\frac{3M_{\text{JTE}}}{4\pi\rho_{\text{JTE}}} \right)^{1/3} = \left(\frac{3}{4} \frac{c_4 G M_{\text{JTE}}}{\Omega_f^2} \right)^{1/3}, \quad (12)$$

and

$$\frac{\Omega_f^2}{\pi G \rho_{\text{JTE}}} = c_4. \quad (13)$$

The orbital angular momentum is given by

$$J_{\text{orbit}} = \Omega_f (M_{\text{COF}} r_{\text{COF}}^2 + M_{\text{JTE}} r_{\text{JTE}}^2), \quad (14)$$

where

$$r_{\text{COF}} = \frac{M_{\text{JTE}}}{M_{\text{CO}}} r_{\text{inner}}, \quad r_{\text{JTE}} = \frac{M_{\text{COF}}}{M_{\text{CO}}} r_{\text{inner}}, \quad (15)$$

are the components' distance to the center of mass, and from Kepler's third law, we obtain their separation

$$r_{\text{inner}} = r_{\text{COF}} + r_{\text{JTE}} = \left(\frac{G M_{\text{CO}}}{\Omega_f^2} \right)^{1/3}. \quad (16)$$

In Eqs. (15) and (16), we used the mass conservation equation (6).

Using Eq. (7), given the CO core rotation period, its mass, the mass of the fission products, and their location on the equilibrium sequences, we can determine the angular velocity of the new binary system, Ω_f , so the corresponding period, P_f . Subsequently, using Eq. (16), we obtain the separation of the fission products, r_{inner} . In the examples shown in Table 2, the new CO core is a Maclaurin spheroid of eccentricity $e = 0.8$, so $c_1 = 0.29345$ and $c_2 = 0.36316$ (see Table 2), and the JTE has a semi-major axis ratio $a_2/a_1 = 0.92$, so $c_3 = 0.304602$ and $c_4 = 0.37319$ (see Table 1).

It is worth noting that Ω_f is greater than Ω , so the angular velocity increases after the fission. In all selected examples, $P_f \lesssim P/2$. Additionally, all fission products exhibit higher density compared to the CO core before fission, i.e., $\rho < \rho_{\text{COF}}$ and $\rho < \rho_{\text{JTE}}$. Another important feature is that the inner binary separation is approximately equal to the sum of the average radii of the fissioned CO core and the JTE, denoted as \bar{a}_{COF} and \bar{a}_{JTE} , respectively, i.e., $r_{\text{inner}} \approx \bar{a}_{\text{COF}} + \bar{a}_{\text{JTE}}$.

4. DISCUSSION AND CONCLUSIONS

Table 2. Fission examples for products that are not at the bifurcation point. From left to right, the columns of the table are the spin period and mass of the initial CO core, the mass of the new CO core, the mass of JTE, the spin period of the fission products, the density of the new CO core and the JTE, the distance between two fission products, the average radius of the new CO core and the JTE.

P (min)	M_{CO} (M_{\odot})	$M_{\text{CO}f}$ (M_{\odot})	M_{JTE} (M_{\odot})	P_f (min)	$\rho_{\text{CO}f}$ (g cm^{-3})	ρ_{JTE} (g cm^{-3})	r_{inner} (cm)	$\bar{a}_{\text{CO}f}$ (cm)	\bar{a}_{JTE} (cm)
110	10	8.5	1.5	50.7241	56.0085	54.5032	6.77722×10^{10}	4.16145×10^{10}	2.35548×10^{10}
90	10	8.5	1.5	41.5016	83.6669	81.4182	5.92859×10^{10}	3.64036×10^{10}	2.06053×10^{10}
40	10	8.5	1.5	18.4452	423.562	412.178	3.45274×10^{10}	2.1201×10^{10}	1.20003×10^{10}
20	10	8.5	1.5	9.22255	1694.27	1648.73	2.17508×10^{10}	1.33558×10^{10}	7.55968×10^9
5	10	8.5	1.5	2.30565	27108.	26379.4	8.63185×10^9	5.30025×10^9	3.00007×10^9

In the context of the BdHN model of GRB-SNe, we have given examples of an alternative scenario to the core collapse of the CO star. The corotation with the NS companion leads the CO star to fission into a new CO core in the Maclaurin sequence and a JTE of smaller mass. We have given examples where an initial CO core of $10M_{\odot}$ splits into a new Maclaurin spheroid CO core of $8.5M_{\odot}$ and a JTE of $1.5M_{\odot}$ (see Tables 1 and 2).

The subsequent evolution of the new CO core in this scenario could potentially provide an alternative SN mechanism: during its collapse, the rotational and magnetic energies of the CO core increase, becoming sufficiently large to unbind the outermost stellar layers or even to disrupt the CO core (Rueda, Ruffini, and Zhang, in preparation).

The evolution of the JTE possibly into a ν NS remains to be studied. If angular momentum is conserved in that process, the parameters of the systems presented here would lead to a ν NS that explains the observations of the X-ray luminosity observed in the very early phases of three BdHNe: GRB 220101A at cosmological redshift $z = 4.2$, GRB 090423 at $z = 8.2$ and GRB 090420B at $z = 9.4$ (Rueda, Ruffini, and Zhang, in preparation; Carlo Bianco et al. (2023)). The transition of the ν NS from the Jacobi to the Maclaurin sequence releases a large amount of energy in kHz gravitational waves that could be detectable by the Advanced LIGO and Virgo interferometers for sources located up to ~ 100 Mpc (see Rueda et al. 2022c, for details).

- 1 We are grateful for the fruitful discussions with Jorge
- 2 Rueda, Bianco Bianco, Yu Wang, M. Della Valle, and
- 3 Rahim Moradi in preparing the manuscript.

APPENDIX

A. EQUILIBRIUM PROPERTIES ALONG THE MACLAURIN AND JACOBI SEQUENCES

We start by generalizing the classical tables of the Maclaurin and Jacobi sequences in Chandrasekhar (1969) (Table I and Table IV) or Jeans (1929) (Table XVI and Table XVII) treatises by extending to physical quantities necessary to describe the process involving fission and evolution of the Maclaurin and Jacobi sequence that can explain the observations of the X-ray luminosity of BdHNe (Rueda, Ruffini, and Zhang, in preparation). The main differences lie in the physical quantities required to describe the dynamics of these systems. This includes the dimensionless expressions of the moment of inertia (I) and the rotational kinetic energy (E_k), both of which are functions of the rotational period (P). These quantities are crucial in formulating the overall energetics of the systems. For more detailed information, see Tables 3 and 4.

REFERENCES

- Aimuratov, Y., Becerra, L. M., Bianco, C. L., et al. 2023,
arXiv e-prints, arXiv:2303.16902,
doi: 10.48550/arXiv.2303.16902
- Becerra, L., Bianco, C. L., Fryer, C. L., Rueda, J. A., &
Ruffini, R. 2016, ApJ, 833, 107,
doi: 10.3847/1538-4357/833/1/107

Table 3. Properties of the Jacobi ellipsoids. The columns from left to right include the following ratios and dimensionless quantities: the ratio of the semi-axes a_2 to a_1 (with rotation along the a_3 axis), the ratio of the semi-axes a_3 to a_1 , the ratio of the average radius to the semi-axis a_1 , the dimensionless square of the angular velocity, the dimensionless rotation period, the dimensionless angular momentum, the dimensionless moment of inertia, and the dimensionless rotational kinetic energy.

a_2/a_1	a_3/a_1	\bar{a}/a_1	$\Omega^2/(\pi G\rho)$	$P/(\pi G^{-1}\rho^{-1})^{\frac{1}{2}}$	$L/(GM^3\bar{a})^{\frac{1}{2}}$	$I/(M\bar{a}^2)$	$E_k/(GM^2\bar{a}^{-1})$
1.00	0.582724	0.835259	0.374230	3.26934	0.303751	0.573347	0.080461
0.96	0.570801	0.818311	0.373980	3.27044	0.303959	0.573932	0.080490
0.92	0.558330	0.800866	0.373190	3.2739	0.304602	0.575754	0.080575
0.88	0.545263	0.782882	0.371785	3.28008	0.305749	0.579013	0.080726
0.84	0.531574	0.764330	0.369697	3.28933	0.307467	0.583909	0.080951
0.80	0.517216	0.745168	0.366837	3.30212	0.309837	0.590699	0.081259
0.76	0.502147	0.725351	0.363114	3.31901	0.312956	0.599696	0.081659
0.72	0.486322	0.704832	0.358424	3.34065	0.316938	0.611287	0.082162
0.68	0.469689	0.683554	0.352649	3.3679	0.321923	0.625965	0.082780
0.64	0.452194	0.661457	0.345665	3.40175	0.328081	0.644351	0.083524
0.60	0.433781	0.638470	0.337330	3.44352	0.335618	0.667248	0.084406
0.56	0.414386	0.614513	0.327493	3.49485	0.344796	0.695714	0.085441
0.52	0.393944	0.589494	0.315989	3.5579	0.355941	0.731158	0.086639
0.48	0.372384	0.563306	0.302642	3.63551	0.369473	0.77551	0.088013
0.44	0.349632	0.535823	0.287267	3.73153	0.385940	0.831469	0.089570
0.40	0.325609	0.506896	0.269678	3.8513	0.406073	0.902923	0.091312
0.36	0.300232	0.476343	0.249693	4.00246	0.430872	0.995668	0.093229
0.32	0.273419	0.443942	0.227153	4.19634	0.461750	1.11871	0.095294
0.28	0.245083	0.409409	0.201946	4.45054	0.500777	1.28676	0.097446
0.24	0.215143	0.372374	0.174052	4.79392	0.551140	1.52543	0.099564
0.20	0.183524	0.332334	0.143610	5.27761	0.618069	1.88328	0.101421
0.16	0.150166	0.288556	0.111044	6.00181	0.710927	2.46347	0.102582
0.12	0.115038	0.239887	0.077281	7.19438	0.848770	3.52552	0.102171
0.08	0.078166	0.267729	0.044168	9.51648	1.079302	5.93005	0.098219
0.04	0.039688	0.116656	0.015415	16.1086	1.58276	14.7202	0.085092
0	0	0	0	∞	∞	∞	

- Becerra, L., Ellinger, C. L., Fryer, C. L., Rueda, J. A., & Ruffini, R. 2019, *ApJ*, 871, 14, doi: [10.3847/1538-4357/aaf6b3](https://doi.org/10.3847/1538-4357/aaf6b3)
- Becerra, L. M., Moradi, R., Rueda, J. A., Ruffini, R., & Wang, Y. 2022, *PhRvD*, 106, 083002, doi: [10.1103/PhysRevD.106.083002](https://doi.org/10.1103/PhysRevD.106.083002)
- Chandrasekhar, S. 1969, *Ellipsoidal figures of equilibrium*
- Della Valle, M. 2011, *International Journal of Modern Physics D*, 20, 1745, doi: [10.1142/S0218271811019827](https://doi.org/10.1142/S0218271811019827)
- Fryer, C. L., Oliveira, F. G., Rueda, J. A., & Ruffini, R. 2015, *Physical Review Letters*, 115, 231102, doi: [10.1103/PhysRevLett.115.231102](https://doi.org/10.1103/PhysRevLett.115.231102)
- Fryer, C. L., Rueda, J. A., & Ruffini, R. 2014, *ApJL*, 793, L36, doi: [10.1088/2041-8205/793/2/L36](https://doi.org/10.1088/2041-8205/793/2/L36)
- Galama, T. J., Vreeswijk, P. M., van Paradijs, J., Kouveliotou, C., & et al. 1998, *Nature*, 395, 670, doi: [10.1038/27150](https://doi.org/10.1038/27150)
- Heger, A., Fryer, C. L., Woosley, S. E., Langer, N., & Hartmann, D. H. 2003, *ApJ*, 591, 288, doi: [10.1086/375341](https://doi.org/10.1086/375341)
- Hjorth, J., & Bloom, J. S. 2012, *Cambridge Astrophysics Series*, Vol. 51, *The Gamma-Ray Burst - Supernova Connection*, ed. C. Kouveliotou, R. A. M. J. Wijers, & S. Woosley (Cambridge University Press (Cambridge)), 169–190
- Jeans, J. 1929, *Astronomy and cosmogony* (CUP Archive)
- Kobulnicky, H. A., & Fryer, C. L. 2007, *ApJ*, 670, 747, doi: [10.1086/522073](https://doi.org/10.1086/522073)
- Moradi, R., Rueda, J. A., Ruffini, R., & Wang, Y. 2021, *A&A*, 649, A75, doi: [10.1051/0004-6361/201937135](https://doi.org/10.1051/0004-6361/201937135)
- Rueda, J. A., Li, L., Moradi, R., et al. 2022a, *ApJ*, 939, 62, doi: [10.3847/1538-4357/ac94c9](https://doi.org/10.3847/1538-4357/ac94c9)
- Rueda, J. A., & Ruffini, R. 2012, *ApJL*, 758, L7, doi: [10.1088/2041-8205/758/1/L7](https://doi.org/10.1088/2041-8205/758/1/L7)
- . 2020, *European Physical Journal C*, 80, 300, doi: [10.1140/epjc/s10052-020-7868-z](https://doi.org/10.1140/epjc/s10052-020-7868-z)
- Rueda, J. A., Ruffini, R., & Kerr, R. P. 2022b, *ApJ*, 929, 56, doi: [10.3847/1538-4357/ac5b6e](https://doi.org/10.3847/1538-4357/ac5b6e)
- Rueda, J. A., Ruffini, R., Li, L., et al. 2022c, *PhRvD*, 106, 083004, doi: [10.1103/PhysRevD.106.083004](https://doi.org/10.1103/PhysRevD.106.083004)
- Ruffini, R., Karlica, M., Sahakyan, N., et al. 2018a, *ApJ*, 869, 101, doi: [10.3847/1538-4357/aaeac8](https://doi.org/10.3847/1538-4357/aaeac8)
- Ruffini, R., Wang, Y., Aimuratov, Y., et al. 2018b, *ApJ*, 852, 53, doi: [10.3847/1538-4357/aa9e8b](https://doi.org/10.3847/1538-4357/aa9e8b)
- Ruffini, R., Moradi, R., Rueda, J. A., et al. 2019, *ApJ*, 886, 82, doi: [10.3847/1538-4357/ab4ce6](https://doi.org/10.3847/1538-4357/ab4ce6)
- . 2021, *MNRAS*, 504, 5301, doi: [10.1093/mnras/stab724](https://doi.org/10.1093/mnras/stab724)
- Sana, H., de Mink, S. E., de Koter, A., et al. 2012, *Science*, 337, 444, doi: [10.1126/science.1223344](https://doi.org/10.1126/science.1223344)
- Smartt, S. J. 2009, *ARA&A*, 47, 63, doi: [10.1146/annurev-astro-082708-101737](https://doi.org/10.1146/annurev-astro-082708-101737)
- . 2015, *PASA*, 32, e016, doi: [10.1017/pasa.2015.17](https://doi.org/10.1017/pasa.2015.17)
- Wang, Y., Rueda, J. A., Ruffini, R., et al. 2022, *ApJ*, 936, 190, doi: [10.3847/1538-4357/ac7da3](https://doi.org/10.3847/1538-4357/ac7da3)
- Woosley, S. E., & Bloom, J. S. 2006, *ARA&A*, 44, 507, doi: [10.1146/annurev.astro.43.072103.150558](https://doi.org/10.1146/annurev.astro.43.072103.150558)

Table 4. Properties of the Maclaurin spheroids. The columns from left to right include the following dimensionless quantities: the eccentricity, $e^2 = 1 - (a_3/a_1)^2$, where a_1 and a_3 are the semi-major axes with rotation along the a_3 axis, the dimensionless square of the angular velocity, the dimensionless rotation period, the dimensionless angular momentum, the dimensionless moment of inertia, and the dimensionless rotational kinetic energy.

e	$\Omega^2/(\pi G \rho)$	$P/(\pi G^{-1} \rho^{-1})^{\frac{1}{2}}$	$L/(GM^3 \bar{a})^{\frac{1}{2}}$	$I/(M \bar{a}^2)$	$E_k/(GM^2 \bar{a}^{-1})$
0	0	∞	0		0
0.10	0.00534	27.369	0.02539	0.4012	0.000803
0.15	0.01204	18.2271	0.03829	0.402941	0.001819
0.20	0.02146	13.6526	0.05144	0.405467	0.003263
0.25	0.03363	10.906	0.06491	0.408712	0.005154
0.30	0.04862	9.07032	0.07882	0.412761	0.007526
0.35	0.06647	7.75742	0.09329	0.417822	0.010415
0.40	0.08727	6.77014	0.10846	0.423942	0.013874
0.45	0.11108	6.00084	0.12450	0.431341	0.017968
0.50	0.13799	5.38401	0.14163	0.440251	0.022781
0.55	0.16807	4.87848	0.16013	0.451021	0.028426
0.60	0.20135	4.45712	0.18037	0.464149	0.035046
0.65	0.23783	4.10107	0.20286	0.480322	0.042838
0.70	0.27734	3.79773	0.22834	0.500663	0.052070
0.75	0.31947	3.53847	0.25792	0.526914	0.063125
0.80	0.36316	3.3188	0.29345	0.562282	0.076574
0.81	0.37190	3.27957	0.30153	0.570935	0.079624
0.81276	0.37423	3.26934	0.30375	0.573345	0.080461